KfK 5385
November 1994

A Model for Numerical Simulation of Devolatilization and Combustion of Waste Material in Packed Beds

B. Peters
Institut für Angewandte Thermo- und Fluiddynamik

Kernforschungszentrum Karlsruhe

KERNFORSCHUNGSZENTRUM KARLSRUHE
Institut für Angewandte Thermo- und Fluiddynamik

KfK 5385

A Model for Numerical Simulation of Devolatilization and Combustion of Waste Material in Packed Beds

B. Peters

Kernforschungszentrum Karlsruhe GmbH, Karlsruhe

Kernforschungszentrum Karlsruhe GmbH
Postfach 3640, 76021 Karlsruhe

ISSN 0303-4003

Abstract

The objective of this paper is to present a numerical simulation method for the calculation of an unsteady, three-dimensional flow and combustion phenomena in a packed bed of a furnace. The entire arrangement of a furnace partly filled with solid particles is separated into a gas phase and a solid phase. The gas flow within the void space between particles is approximated by flow through porous media according to Darcy's law. The outer flow region of the combustion chamber will be modelled as a laminar/turbulent viscous flow. Therefore a set of equations, i.e. continuity, momentum and energy equation including the homogeneous combustion between a gaseous fuel and air are applied to describe accurately the behaviour of the phenomena encountered.

The motion of the solid phase, as a flow of one particle past another, is accounted for by particle-to-particle friction. As heating up and combustion of particles significantly changes their size, temperature and composition this behaviour is treated by a special particle modelling step. It takes into account a size reduction due to heterogeneous combustion, non-uniform temperature distribution due to internal heat generation and both convective and radiative heat transfer within the gas phase and the solid phase, and a varying composition due to pyrolysation and gasification. Similar to the gas phase, a set of conservation equations applied to particles yields the solution for the relevant variables.

The sets of equations for both the solid and the gas phases will be solved by a time-marching finite volume approach on an unstructured computational mesh with arbitrarily shaped cells. This novelty enhances body fitted meshing and resolution of high gradient domains. An efficient non-iterative solution algorithm is employed, which allows the size of the computational time step to be controlled solely by accuracy, rather than numerical stability, considerations in the interest of economy.

The method is assessed by application to two different furnace geometries, for which a wide range of experimental data, e.g. temperature, flow rates, and species measurements are available.

Ein Modell zur numerischen Simulation der Pyrolyse und Verbrennung von Abfallstoffen im Festbett

Kurzfassung

Innerhalb des vorliegenden Berichts wird eine numerische Simulationsmethode vorgestellt, um die instationäre, dreidimensionale Strömung und Verbrennung von Partikeln in einem Festbett eines Ofens zu berechnen. Die Anordnung besteht aus einem Verbrennungsraum, der teilweise mit Feststoffpartikeln gefüllt ist. Die Strömung in den Freiräumen zwischen den Partikeln wird als Strömung durch ein poröses Medium beschrieben, auf die das Gesetz von Darcy angewendet werden kann. Der verbleibende gasförmige Verbrennungsraum wird als laminare/turbulente, reibungsbehaftete Strömung simuliert und kann durch die Kontinuitäts-, Impuls- und Energiegleichung einschließlich homogener Verbrennung zwischen einem gasförmigen Brennstoff und Luft beschrieben werden.

Die Bewegung der Feststoffpartikel resultiert aus einer Bilanz zwischen Reibungskräften an den Berührungspunkten der Partikel und von außen einwirkenden Kräften. Da während der Aufheizphase und hauptsächlich während der Verbrennung der Partikel sich ihre Größe, Temperatur und Zusammensetzung ändern, wurde ein effizientes Verfahren zur Beschreibung dieser Parameter entwickelt. Damit wird der Masseverlust durch Verbrennung, ungleichmäßige Temperaturverteilung als Folge von Wärmefreisetzung und Wärmetransport hervorgerufen durch Konvektion und Wärmestrahlung als auch die sich ändernde Zusammensetzung mit fortschreitender Pyrolyse und Vergasung erfaßt. Analog zur Gasphase werden auch hier Kontinuitäts-, Impuls- und Energiegleichung zur Lösung der relevanten Variablen benutzt.

Die Gleichungen sowohl für die Gas- als auch die Feststoffphase werden auf einem unstrukturierten Gitter mit beliebiger Zellgeometrie mit einer instationären Finite-Volumen-Methode gelöst. Dieser Ansatz ermöglicht körperangepaßte Gitter und die Auflösung von Gebieten mit hohen Gradienten. Ein nicht-iterativer Algorithmus, bei dem der Zeitschritt nur durch numerische Genauigkeit und nicht durch Stabilitätskriterien bestimmt wird, ermöglicht ökonomische Rechenzeiten.

Berechnungen mit dem Modell werden an zwei verschiedenen Ofengeometrien durchgeführt, für welche eine große Anzahl experimenteller Daten wie Temperatur, Masseströme und Konzentrationsmessungen vorliegen.

Contents

1 Introduction

During recent years a significant improvement in understanding different aspects of combustion has been achieved, driven by the continuing search for better performance combined with lower levels of pollution of such systems. Impressive advances in both numerical modelling and experimental techniques have provided a better insight into the fundamental aspects of combustion phenomena and have made designs for practical applications more reliable. Within this chapter a survey of combustion and related phenomena, e.g. flow, mass and heat transfer will be given. As the treatment of combustible waste material is still a rather young field of research not too well understood, only very limited experience has been gained. Therefore this survey is directed more at char and coal combustion in conjunction with other materials such as wood, whith a longer history of research. In how far these methods can be applied to the problem dealt with in this presentation will be shown. In general, the principles for char/coal and waste material combustion resemble each other to a large extend and can be subdivided into three major stages: heating-up, pyrolysis with devolatilization, heterogeneous and homogeneous combustion [36], [41].

1.1 Devolatilization

As decomposition during devolatilization and pyrolysis is a very complicated and complex process, dependent also on heat transfer by convection and radiation; some tentative first models were based on a global one-dimensional energy balance, as employed by Wichman [59]. They were concentrated on determining the evolution rate of volatile gas and the surface temperature of the pyrolyzing sample. Together with a one-dimensional formulation to the energy equation, they applied a global one-step reaction mechanism for the decomposition process. The influence of a flow field and, hence convective heat transfer was neglected and radiation was the only means of transfer accounted for. Thus four different stages were identified during devolatilization of wood, i.e. inert heating, initial pyrolysis, thin char and finally a reaction front traveling into the wood to form an outer hot char region. Furthermore while the wavelike nature of the process was recognized it was admitted that the model could be made more realistic by the addition of effects of moisture and of char oxidation.

These disadvantages were compensated to some extent by the work by Laraqui and Bransier [47]. They took into account effects of moisture during heating-up and added convective heat transfer as well. Again based on a one-dimensional form of the energy equation and decomposition described by a one-step exothermic reaction of an Arrhenius form served as a basis for comparing results obtained from this model with experiments on PMMA (polymethylmethacrylate). Their comparison for time-dependent surface temperature and volatile flux due to pyrolysis and devolatilization led to good agreement indicating that this simplified approach can be used to describe the process of pyrolysis.

A more detailed investigation into the effect of heat transfer on coal devolatilization was carried out by Yang and Wang [33]. They examined both radiative and convective heat transfer effects on the transient behaviour of preheating, ignition, and combustion of a single particle pyrolyzing in a hot environment. The solid phase consists of an unreacted core, a pyrolyzing zone and a charred layer. One-dimensional conservation equations in a

cylindrical reference frame were applied to the solid and gaseous phases inside and around the porous particle. The rate of pyrolysis is calculated according to a competitive two-step reaction mechanism accounting for slow and fast kinetics, as suggested also by Kobayashi [28]. Devolatilized products were transported through porous layers of particles and mixed with surrounding air at the surface, where they are converted within a flame sheet around the particle within the gas phase. For most of their comparisons with experimental data reasonably good agreement was achieved discrepancies being attributed to char cracking and thus surface increase and combustion rate enhancement. However, for a Reynolds number Re < 40 and millimeter-sized particles they confirmed the shift from kinetically to diffusion controlled reactions with increasing temperature. Besides radiation from flames wall radiation was the dominating effect throughout the whole combustion process.

Niksa and Lau [58] started from two very sophisticated and specially tailored models to predict the devolatilization rates of coal. Complexity and CPU time consumption made them replace these by a more manageable Distributed Activation Energy Model (DAEM) again based on a one-step reaction mechanism. Comparison of the three models shows that the simplified model captured equally well the behaviour of devolatilization at various heating-up rates and also predicted the shift in the frequency factors by about a factor of 6 for a change in the heating rate by one order of magnitude.

A continuous Gaussian distribution of activation energies was also assumed by Anthony et al. [4] and led to good agreement with experimental data on the devolatilization rates for char [45], [42].

Very useful data about waste material are reported by Tchobanoglons and Theisen [22]. These data contain amounts of devolatiles during pyrolysis and the fraction dependent on temperature as shown in Table 1 and 2.

Temperature K	Volatiles kg/kg waste
755	0.123
921	0.186
1088	0.237
1199	0.244

Table 1: Volatile products of municipal solid waste

Models of a one-dimensional formulation including a one-step reaction mechanism with radiative and convective heat transfers seem to be in good agreement with experimental data and therefore should be transferable to waste material combustion.

1.2 Ignition

As particles are heated in exothermic reactions during devolatilization and due to heat transfer conditions will eventually be reached at which ignition occurs. However, no general ignition conditions have been identified or have been adequately described or correlated so far [66]. Usually ignition is said to occur when a selt-sustaining reaction

Component	Temperature K			
% Vol.	755	921	1088	1199
H_2	5.56	16.58	28.55	9.26
CH_4	12.43	15.91	13.73	10.45
CO	33.5	30.49	34.12	35.25
CO_2	44.77	31.78	20.59	18.31
C_2H_4	0.45	2.18	2.24	2.43
C_2H_6	3.03	3.06	0.77	1.07

Table 2: Composition of volatile gas

of a fuel and an oxidizer is initiated or a visible flame is seen. Ignition in a two-phase system can occur in a homogeneous manner within the gas phase or on the surface of a solid particle [26]. Heat generated by this initial process will enhance and accelerate combustion and eventually may lead to a run-away condition.

Kashiwagi [60] examined six different ignition criteria. In conjunction with one-dimensional conservation equations for energy and species applied to the solid and gaseous phases he decided on a criterion in which the total gas phase reaction rate becomes equal to or larger than a given value. From several parametric studies he concluded that a gas phase reaction must be included in the model and that heat adsorption of the particle has an impact on ignition delay time. Furthermore the exothermicity or endothermicity of pyrolysis does not greatly effect radiative ignition and there are upper and lower limits of the the pyrolysis activation energy for ignition at given values of the gas phase activation energy and the frequency factor. These findings were corroborated by Kashiwagi [61] in a later investigation which showed that three major terms i.e. conduction into a sample, radiation and endothermic decomposition account for most (78 %) of the energy loss in the case of PMMA.

Evidence of ignition first occuring in the gas phase is also provided by Essenhigh et al. [26] who suggests a regime of homogeneous ignition for particles greater than 100 microns [17] [27]. In his review he identifies seven commonly used criteria for ignition. Within his investigation he applies a one-dimensional transient energy equation and modifies the Semenov condition [48] for ignition in a way such that the heat- generating term has to be bigger than, instead of equal to, the heat losses. Comparisons with experiments showed good agreement for gas temperatures at ignition as a function of particle diameter for different char and coal.

A similar approach was taken by Di Blasi [18] who calculated fuel, oxidizer and temperature curves for both the gaseous and the solid phases on the basis of a one-dimensional unsteady formulation of conservation equations. From these calculations in conjunction with experimental data ignition was assumed to occur when the time-gradient of temperature exceeded a value of 8000 K/s. Ignition delay times were compared to data by Kashiwagi and led to a reasonably good agreement. Predictions for horizontally mounted as opposed to vertically mounted samples present a qualitatively better match with experiments. The discrepancies are attributed to a lack of convection and two-dimensionality.

Fu and Zhang [7] compared their ignition criteria, with the first and second time derivative having to vanish, with measured temperature histories of small char and coal particles of different compositions. The predictions of the ignition temperature were within an error of 10%. However, the error for the predicted ignition delay times was larger.

These results altogether highlight once more the difficulties in determining unique ignition criteria. On these grounds none of these criteria can be recommended unequivocally for application in waste combustion.

1.3 Combustion

An ignition process either homogeneous within a surrounding gas phase or on a solid surface is usually considered to be the onset of combustion, with the homogeneous ignition regime valid for particles bigger than 100 microns in diameter [26]. As opposed to the latter mode heterogeneous ignition starts combustion on a surface and then may increase the devolatilization rate significantly. Eventually volatile matter will also combust homogeneously and the fastest of these two competitive combustion processes will determine the general behaviour. Evidently two basically different combustion modes must be considered - homogeneous and heterogeneous combustion as reviewed in this chapter. Again as municipal waste material (MWM) combustion is a very young discipline in research the section below focuses on work done mainly within the field of coal and char combustion thus identifying methods applicable to waste material combustion.

1.3.1 Combustion of Solid Particles

Howard et al [9] contributed to the clarification of solid-particle combustion by elucidating simultaneous gas-phase volatile combustion. Experiments carried out with particles of less than 200 micrometer diameter proved their assumptions right. After ignition heterogeneous combustion occurs for a brief period during which basically no devolatilization takes place. The end of this period is marked by rapid volatile evolution and burning of volatiles occurs simultaneous with heterogeneous combustion. An unsteady combustion model adopted from the theory of oil drop combustion defines a radius of a reaction zone around spherical particles and was employed to investigate the effect of particle size on combustion. Thus in conjunction with experimental data a critical particle radius was identified above which the volatile mass flux is sufficient for a reaction zone detached from the solid surface and hence prevent access of oxygen to a particle and heterogeneous combustion. For a particle diameter below the critical value both modes of combustion occur the rate on the surface depending on the oxygen available and not consumed by gas phase combustion. Furthermore they concluded that the rate of heterogeneous burning is controlled by the rate of the chemical reaction rather than by the rate of mass transfer.

Petrella [64] applied a global unsteady energy balance equation including radiation from flames and external walls, reaction enthalpy for gasification and heat losses to evaluate mass burning rates of polymers, wood and organic liquids. With the weight loss during combustion obtained experimentally the burning rate and the heat flux to gasify and pyrolyse different materials was predicted.

While investigations mentioned above concentrated more on a phenomenological description of the combustion process Loewenberg and Levendis [44] included effects of pore diffusion and growth, inert mineral matter, gas phase heat and mass transfer. Time-dependent one-dimensional equations for the particle temperature, the radius and the ash layer thickness describe the combustion dynamics. These equations are coupled with conservation equations for gas-phase transport. The conversion of solid products into CO is accounted for by a one-step reaction with oxygen. On the basis of experimental results char was characterised by particle size, morphology, density and pore structure as part of the simulation. In conjunction with these parameters, the intrinsic rate of the reaction process was evaluated. Comparison with a simpler model [2] revealed that predicted intrinsic rates differed by a factor of 5-8 due to gas phase properties and pore enlargement. The estimated rates were used to calculate temperature profiles which were found to be in good agreement with experimental data.

A similar experimental and modelling study of cellulosic char combustion under laminar flow conditions was carried out by Smith, Pendarvis and Rice [21]. They sought to develop an integral reactor model that fitted the combustion rates of a thermogravimetric furnace in a temperature range of 473-1173 K with 0.03-0.21 oxygen mole fraction. But unlike the previous authors, who had stated that reactions were chemically controlled they developed a mass transfer controled model and hence assumed the char oxidation reaction to occur instantaneously. Results of a one-dimensional unsteady transport equation, mass transfer dependent on the Sherwood number correlated with experimental data with an error margin of 11%. From these results the authors inferred that the reaction zone does not penetrate into the porous char to any appreciable extent.

Blake and Libby [51] worked out a theory of the quasi-steady behaviour of a single carbon particle in a slow viscous flow of an oxidizing gas. Application of the conservation equations to a spherical particle furnished solutions for the stream function, species mass fraction and enthalpy. The Prandlt and Schmidt numbers were set equal to unity and the system of equations together with the appropriate boundary and initial conditions was solved by asymptotic expansions. Both local and integral mass loss rates for burning a particle were derived. The configuration and distortion of a flame sheet around a particle due to a flow field were discussed. Unfortunately no comparison with experimental data was presented.

Another study emphasizing the importance of oxygen chemisorption kinetics on coal and char for the combustion process was conducted by Khan, Everitt and Lui [53]. The chemisorption of oxygen is important in evaluating auto-ignition and in investigating the process of heterogeneous combustion. Experiments measuring the chemisorption of oxygen for coal particles 24 μm in size were carried out with a thermogravimetric analyzer over a temperature range of $100^o - 225^oC$. For better understanding of the process the validities of various one-dimensional and unsteady models in predicting chemisorption rates were tested. One of them the Elovich equation is a model commonly used in adsorption studies and describes the relationship between the rate and the amount of oxygen uptake as follows:

$$\frac{dc_{O_2}}{dt} = a\, exp(-\alpha c_{O_2}) \tag{1}$$

where a and α are empirical constants. Comparison with their experimental data showed that no fit could be achieved with a single set of constants a and α. Similar results that the model broke down in distinct regions were also reported by Bansal, Vastola and Walker [10], Low [15] and Taylor and Thon [3]. The second model with an Arrhenius equation revealed the activation energy to increase from 4-63 kJ/gmol with rising temperature and additionally to depend on the site coverage with oxygen.With the shift of activation energy taken into account it was proposed that chemisorption is influenced to a large extent by diffusion processes. A shrinking-area model which allowed oxygen to access freely available surface area without any limits on diffusion also was incapable of predicting the time-dependent oxygen uptake. Finally a diffusion model was tested which showed good agreement with the adsorption data. However, errors in the early stage of chemisorption may be quite large. Therefore the authors concluded that in an early phase the Elovich equation represents a good approximation whereas the later stage is better represented by the parabolic diffusion law.

The existence of different regimes had already been postulated by Walker, Rusinko and Austin [50] and by Gray, Cogoli and Essenhigh [14]. They subdivided the regime of controlling resistance of which the first zone is controlled by the chemical reaction for low temperatures or small particles. Zone II is characterized by control due to both chemical reaction and pore diffusion. Within zone III for high temperatures mass transfer limitations become predominant. These investigations highlighted the importance of intrinsic rate modelling as opposed to global rate modelling which neglects the following aspects of chared coal particles:

1) pyrolysis during char oxidation
2) changes in pore structure
3) internal diffusion
4) internal chemical reaction

Articles and reviews [43], [67], [25] also stressed intrinsic rate modelling; despite of the difficulty of developing an adequate model it allows the greatest potential for differentiation among various rate-influencing parameters.

These results were supported by Specht [19], who identifies heat conduction, heat and mass transfer, pore diffusion and chemical kinetics as predominant mechanisms in heterogeneous combustion. Based on unsteady conservation equations for energy and for species for a sphere and a slab geometry he compared predictions with experimental results for the combustion of coal, reduction of iron ore and decomposition of limestone and dolomite. The results showed that for a temperature of less than $1000°C$ the diffusion process was strongly temperature-dependent and could be approximated by an Arrhenius equation. Sorption, desorption and the surface reaction were approximated by a Langmuir-Hinshelwood isotherm.

One recommendation to be made in the case of waste material combustion seems to be that due to similar material structures and combustion behaviour intrinsic rate modelling cannot be circumvented despite the effort that must be invested.

1.3.2 Combustion of Volatiles

A variety of products emerge during devolatilization, among them combustible species such as hydrocarbons (C_nH_m), hydrogen (H_2) and carbonmonoxide (CO) as the major components. In practical applications several hundred hydrocarbon compounds were identified for coal and the situation will be similar for waste materials. Obviously, one cannot treat every single component separately as the combustion process of a single species often comprises hundreds of reactions [55], [57]. Therefore global chemical reaction rates are correlated for H_2, CO and one representative hydrocarbon, the rate for the latter possibly allowing a distinction to be made between chain or cyclic hydrocarbons and fast or slow kinetics.

An approach of this type was proposed by Edelmann and Fortune [6] and Siminski et al [31], in which the reaction products are H_2 and CO rather than H_2O and CO_2 as for a perfectly depleted fuel.

$$C_nH_m + \frac{n}{2}O_2 \rightarrow \frac{m}{2}H_2 + nCO \tag{2}$$

Different rates were applied for long-chained and cyclic hydrocarbons. The coefficients n and m can be determined by a material balance including all hydrocarbons.

Hautman et al [46] supplied overall reaction rates for H_2, CO, C_2H_4 and alkanes.

$$C_nH_{2n+2} \rightarrow \frac{n}{2}C_2H_4 + H_2 \tag{3}$$

$$C_2H_4 + O_2 \rightarrow 2CO + 2H_2 \tag{4}$$

$$CO + \frac{1}{2}O_2 \rightarrow CO_2 \tag{5}$$

$$H_2 + \frac{1}{2}O_2 \rightarrow H_2O \tag{6}$$

This sequence proved to be quite reliable over a temperature range of 960-1540 K and a pressure range of $1 - 9\ N/m^2$.

A global rate for the oxidation of HCN was reported by DeSoete [20], which is important for the formation of NO from fuel nitrogen during combustion.

1.3.3 Changes within Particles during Combustion

As the combustion of waste material proceeds the shape, size and pore volume of particles undergo major changes, as addressed by Shkadinky et al. [65]. Their assumption is based on the fact that increasing pressure within the pore volumes of porous material will lead to an expansion and thus increase the pore volume. Compaction occurs when the pore pressure decreases. The deformation process is modelled by an Arrhenius-like equation including an activation energy and a pre-exponential factor depending on porosity itself. One-dimensional unsteady conservation equations for energy, momentum and species include a one-step reaction mechanism for the combustion of solid material. Their results indicate that substantial porosity changes occur during combustion, with changes in porosity closely related to combustionrate.

1.4 Heat and Mass Transfer

As all processes of heating, devolatilization and heterogeneous combustion are governed largely by heat and mass transfer a method has to be identified to describe the transfer accurately. Obviously treating every single particle plus the boundary layer flow around it exceeds available resources of computer memory and CPU time. Moreover resolving this problem with such an accuracy is beyond the scope of this study. Therefore integral methods describing transfer by heat and mass transfer coefficients respectively will be applied in this study. A wide range of experimental work has already been carried out in this field and the appropriate laws in terms of Nusselt and Sherwood numbers are well established for different geometries and flow conditions. Good compilations can be found in these references [19], [5], [40], [1], [62], [24].

1.5 Radiation

Adequate treatment of heat transfer by thermal radiation is essential in a model of waste material combustion. The contribution by radiation to heat transfer grows with the combustor size and therefore plays a dominant role in industrial furnaces. The level of detail required for radiative transfer depends on whether the instantaneous spectral local radiation flux, flame structure, scalar properties or the formation of particles generated in the flame e.g. soot are to be resolved. Radiation is influenced by several attenuating and weakening effects which, unfortunately are governed by a complex integrodifferential equation [35], [54] with wavelength-dependent terms of the following form:

$$\frac{di_n(\lambda)}{dn} = -a(\lambda)i_n(\lambda) + \epsilon(\lambda)i_{n,b}(\lambda) - \sigma_s(\lambda)i_n(\lambda) + \frac{\sigma_s(\lambda)}{4\pi}\int_{\omega_i=4\pi} i_n(\lambda,\omega_i)\Phi(\lambda,\omega,\omega_i)d\omega_i \quad (7)$$

where the change of intensity i into the direction n is given by the loss by adsorption, the gain by emission, the loss by scattering and the gain by scattering into the direction of radiation.

The divergence of Eq 7 within the energy equation will determine the contribution of radiative transfer to the thermal behaviour of the system. This integrodifferential equation is difficult to solve, which is why simplifications were made to faciliate the solution process. One of these which has often been applied to packed beds replaces the radiative flux by an equation similar to that for heat conduction of the following form:

$$q_r = -k_r\frac{dT}{dn} \quad (8)$$

with the radiant flux q_r expressed by the temperature gradient and an apparent conductivity k_r for radiation.

An approach like this was developed by Chen [11] for packed beds, where the radiative heat flux is expressed by an algebraic equation accounting for the position, bed thickness, boundary emissivities and temperatures and bed properties. Chen and Churchill [12] compared their model with experimental data and found it to be in good agreement.

A similar approach was used by Chan and Tien [34], Vortmeyer [16] and Zehner [49]. Their derivation is restricted to spherical beds and therefore seems only to be of little use for this study. From among the two treatments accounting for radiation within this project Chen's model and a method described in detail in the following chapter "Description of Method" will be employed. The latter method is based on Equation 7 and a solution is obtained by a multiflux model, contained among other solution methods in references [56], [52].

2 Description of the Method

2.1 Introduction

In the following sections the current method for numerical simulation of the flow and the combustion phenomena in a packed bed of a furnace for municipal waste material combustion is described. If a small fraction is extracted from a packed bed it may have the appearance shown in Figure 1.

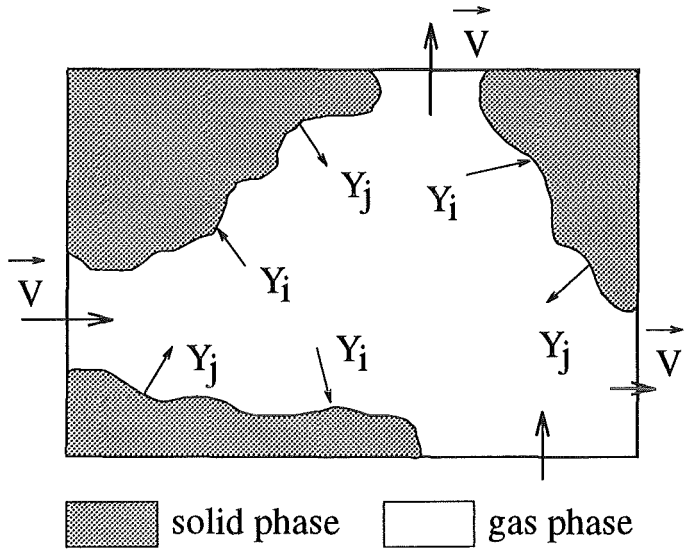

Figure 1: Extraction of a packed bed

Part of the element is made up of solid material, whereas the remaining void volume is occupied by the gas phase. A mass flux of both solid material and gas can cross the boundaries to neighbouring elements. Between the solid phase and the gas phase various mass and heat transfer mechanisms take place which are caused by evaporation, devolatilization and combustion. The gas flow between the particles of the bed is treated as a flow through porous media according to Darcy's law. The motion of particles mainly due to externally applied forces is taken into account. Heat transfer and mass transfer between the gas phase and solid phase are based on similarity analysis validated by experiments. As particles are heated up by radiative fluxes from the furnace walls various processes take place on the particle surface and within the particles. At medium temperatures

water evaporates which is described by an Arrhenius law. At higher temperatures various decompositions into gaseous products are described by appropriate rate expressions.

The set of non-linear differential equations for continuity, momentum and energy are solved by a time-marching finite-volume approach. An implicit and explicit scheme is implemented. However, due to a large variety of time scales e.g. reaction and diffusion time scales inherent in the system the implicit approach is favoured as there is no limitation by the stability criteria of Courant for the smallest time scale. In order to resolve distributions of scalar variables within the solid phase a form of subgrid modelling is implemented for this purpose and hence does not require very refined meshes. This latter feature together with an implicit scheme thus will lead to relatively moderate computation times.

As only limited knowledge of such systems is currently available calculations with the present model will yield detailed information about the flow, devolatilization and combustion process and thus identify relevant process parameters for future designs.

2.2 Equations and Assumptions

2.2.1 Gas Phase

Before establishing a system of equations for the gas phase a phenomenological description of a packed bed dealt with in this study will be given. At the same time this will identify a method for treating the gas flow in such arrangements. In accordance with the sketch in Figure 1 and the general consistency of packed beds of municipal waste material it can be characterized by the following statements:

1) The packed bed consists of solid particles and void space
2) Void space or pores are distributed at random
3) No pores are sealed off
4) The pores are reasonably uniform in size
5) The porosity is not too high
6) Diffusion (slip) phenomena are absent
7) Fluid motion occurs like motion through a batch of capillaries

With this description the hydraulic radius theory of porous media allows flows within such a complicated and randomly arranged network to be treated.

Initial work was carried out by Darcy, who related flows in porous media to the governing pressure gradient through viscosity and porosity as an essential parameter of porous media. Hence the following assumptions are valid for the gas phase: The flow is a three-dimensional viscous flow through a porous medium obeying Darcy's law. However, the law deviates for high Reynolds numbers which require treatment for laminar and turbulent flow regimes divided by a critical Reynolds number $R_{crit.}$.

$$Re = \frac{v\delta}{\nu} \tag{9}$$

with δ as a length based on a characteristic dimension (e.g. $\sqrt{k}$ with k denoting permeability) of the porous media. The gas flow in a porous medium is compressible, and

various transient effects make it an unsteady motion. The momentum due to mass transfer from particle surfaces into the gas phase is negligible. Because of the existence of different components in the flow the gas phase is treated as a perfect mixture of perfect gaseous components to which the equation of state applies.

As combustible products emerging from the surfaces of particles have first to mix with the surrounding air, essentially combustion in the laminar and turbulent flow regimes is assumed to be non-premixed. Therefore an additional equation for the mixture fraction of fuel in air or a flamelet approach would seem to be appropriate to deal with the combustion of gaseous species. However, this analysis is at present beyond the scope of this study. Additionally, devolatilization yields a wide range of different gaseous fuels, which for reasons of complexity cannot be treated separately. Correlations of chemical reaction rates of these fuels lead to a global reaction rates for H_2, H_2O, CO_2, CO and an alkane C_nH_{2n+2}, which makes calculation feasible. Thus the following global reactions in gaseous hydrocarbon flames with their rates of $kmol/m^3s$ are implemented [46] for combustible products.

$$C_nH_{2n+2} \rightarrow \frac{n}{2}C_2H_4 + H_2 \tag{10}$$

$$C_2H_4 + O_2 \rightarrow 2CO + 2H_2 \tag{11}$$

$$CO + \frac{1}{2}O_2 \rightarrow CO_2 \tag{12}$$

$$H_2 + \frac{1}{2}O_2 \rightarrow H_2O \tag{13}$$

$$\frac{d(C_nH_{2n+2})}{dt} = -10^{20.32}exp-\frac{49600}{RT}(C_nH_{2n+2})^{0.5}(O_2)^{1.07}(C_2H_4)^{0.4} \tag{14}$$

$$\frac{d(C_2H_4)}{dt} = -10^{17.7}exp-\frac{50000}{RT}(C_2H_4)^{0.9}(O_2)^{1.18}(C_nH_{2n+2})^{-0.37} \tag{15}$$

$$\frac{d(CO)}{dt} = -10^{17.6}exp-\frac{40000}{RT}(CO)^{1.0}(O_2)^{0.25}(H_2O)^{0.5}\,7.93exp(-2.48\Phi) \tag{16}$$

$$\frac{d(H_2)}{dt} = -10^{16.52}exp-\frac{41000}{RT}(H_2)^{0.85}(O_2)^{1.42}(C_2H_4)^{-0.56} \tag{17}$$

with Φ as the equivalence ratio. Howard [8] gives as a reaction rate for CO oxidation the following expression.

$$\frac{d(CO)}{dt} = -1.3\,10^{17.6}exp-\frac{125540}{RT}(CO)^{1.0}(O_2)^{0.5}(H_2O)^{0.5} \tag{18}$$

Under the assumptions outlined above the resulting set of coupled non-linear differential

equations for mass, momentum, energy and species together with the equation of state are summarised below in Cartesian coordinates.

Continuity:

$$\frac{\partial \rho_g}{\partial t} + \nabla \cdot (\rho_g(\mathbf{v_g} - \mathbf{v_B})) = S_g \tag{19}$$

Here ρ_g and v_g are gas density and velocity at a position and time t respectively and v_B denotes a velocity of a moving boundary. The source term on the right hand side includes mass transfer rates between the solid and the gaseous phases due to devolatilization and heterogeneous combustion.

Momentum:

$$\frac{\partial(\rho_g \mathbf{v_g})}{\partial t} + \nabla \cdot (\rho_g(\mathbf{v_g} - \mathbf{v_B})\mathbf{v_g}) = -\nabla p_g + F(\mathbf{v}) \tag{20}$$

where p_g stands for the gas pressure. The function $F(\mathbf{v})$ accounts for different flow regimes. Experimental measurements [13] have shown that Darcy's law is valid for a Reynolds number based on $\sqrt{k}$ smaller than $\sim$ 10. Above this value inertia effects reminiscent of turbulent flow over a rough surface introduce a non-linear behaviour, which leads to Forchheimer's equation as a modification of Darcy's law.

$$F(\mathbf{v_g}) = \begin{cases} -\frac{\mu}{k}\mathbf{v_g} & \text{if Re<10 (Darcy)} \\ -\frac{\mu}{K}\mathbf{v_g} - \rho_g C \mathbf{v_g} \mid \mathbf{v_g} \mid & \text{if Re}\geq\text{10 (Forchheimer)} \end{cases} \tag{21}$$

where k is the permeability and K and C are constants of the form [39], [38]:

$$K = \frac{d^2 P^3}{150(1-P)^2} \tag{22}$$

$$C = \frac{1.75(1-P)}{dP^3} \tag{23}$$

Species:

$$\frac{\partial(\rho_g Y_{i,g})}{\partial t} + \nabla \cdot (\rho_g(\mathbf{v_g} - \mathbf{v_B})Y_{i,g}) = \nabla \cdot (D_{i,g} \nabla Y_{i,g}) + S_{Y_{i,g}} \tag{24}$$

where $Y_{i,g}$, and $D_{i,g}$ are mass fractions (e.g. H_2, H_2O, CO, CO_2, C_nH_m) and diffusion coefficients of the species Y_i respectively. The source term $S_{Y_{i,g}}$ takes into account mass sources due to evaporation, devolatilization and combustion.

Energy:

$$\frac{\partial(\rho_g e_g)}{\partial t} + \nabla \cdot (\rho_g(\mathbf{v_g} - \mathbf{v_B})e_g) = \nabla \cdot (\lambda_g \nabla T_g) - p\nabla \cdot \mathbf{v_g} - F(\mathbf{v_g})\mathbf{v_g} + \mathbf{\Gamma} \tag{25}$$

Here Γ is the heat loss/gain of the gas and at the walls and heat generation due to chemical reactions.

$$e = c_{v,g} T_g \tag{26}$$

is the specific internal energy, given by the product of constant-volume specific heat $c_{v,g}$ weighted by mass fractions and gas temperature T_g.

Equation of state (for an assumed perfect gas):

$$\frac{p}{\rho} = R\,T \tag{27}$$

where R is the gas constant. The emissive and adsorptive properties of the gas phase are negligible because of short ray traveling distances and low concentrations of H_2O, CO and CO_2.

As a wide temperature range ($300\ K < T < 1500\ K$) is covered and properties thus change considerably temperature dependent properties will be used. For the laminar flow regime the following equations are applied to approximate conductivity, viscosity and specific thermal capacity for different species as a function of temperature [19] with an error margin of $\pm$ 3 %.

$$\frac{cp}{cp_0} = \left(\frac{T}{T_0}\right)^{n_{cp}} \tag{28}$$

$$\frac{\lambda}{\lambda_0} = \left(\frac{T}{T_0}\right)^{n_{\lambda}} \tag{29}$$

$$\frac{\mu}{\mu_0} = \left(\frac{T}{T_0}\right)^{n_{\mu}} \tag{30}$$

Here the indexed values stand for reference values ($T_0 = 273\ K$) together with the exponents according to Table 3.

Alternatively the specific thermal capacity can be approximated by the following formula albeit at the expense of computational expense [36].

$$c_p = a + b\vartheta + c\vartheta^2 + d\vartheta^3 + e\vartheta^4 \tag{31}$$

where $\vartheta = 0.001T$ applies and the constants take the following values as listed in table 4.

The diffusion coefficient for carbon dioxide and hydrogen in air accounts to $D_{CO_2} = 0.16\ cm^2/s$ and $D_{H_2} = 0.611\ cm^2/s$. For water the diffusion coefficient can be approximated by the following relation [62].

$$D_{H_2O} = \frac{82}{p}\left(\frac{T}{T_0}\right)^{1.8} \tag{32}$$

Gas	c_{p0} kJ/kgK	n_{cp}	λ_0 W/mK	n_λ	μ_0 mg/ms	n_μ
H_2	14.2	0.05	0.17	0.69	8.5	0.65
CH_4	2.08	0.59	0.031	1.26	10.6	0.72
H_2O	1.75	0.2	0.016	1.42	8.7	1.13
CO	1.0	0.12	0.024	0.78	16.8	0.67
AIR	1.0	0.1	0.025	0.76	17.4	0.67
CO_2	0.84	0.3	0.017	1.04	14.4	0.77

Table 3: Gas properties

Gas	a	b	c	d	e
CH_4	2.2624	-3.13946	13.4854	-1.1	2.87374
H_2O	1.8573704	0.14084	0.24771	-0.1285	0.2073
CO	1.035797	0.0333	0.13695	-0.09421	0.01939
AIR	1.00186	$7.22153\ 10^{-5}$	$3.48066\ 10^{-7}$	$-3.21086\ 10^{-10}$	$9.30682\ 10^{-14}$
CO_2	0.81995447	0.51054	-0.28936	0.09758	-0.0141

Table 4: Constants for evaluation of the thermal capacity

Here p stands for the total pressure $[N/m^2]$ and $T_0 = 273\,K$ is a reference temperature.

As mentioned above Forcheimer's equation in the momentum and energy equations applies to the turbulent flow regime, hence only the turbulent transport of a scalar quantity remains to be modelled. For this reason Boussinesq's eddy viscosity theory is employed which relates turbulent shear stresses with an apparent turbulent viscosity μ_t to mean flow gradients. Equating Forchheimer's equation with the turbulent stress tensor yields the turbulent viscosity

$$\mu_t = \frac{\rho_g C \mathbf{v_g} \mid \mathbf{v_g} \mid -2\bar{k}}{\nabla^2 \cdot \mathbf{v_g}} \tag{33}$$

where $\bar{k}$ is the turbulent kinetic energy and in this case is negligible compared to the velocity squared.

Finally turbulent transport of the species $Y_{i,g}$ will result in the following equation.

$$j_{Y_{i,g},t} = \frac{\mu_t}{\sigma_t} \nabla Y_{i,g} \tag{34}$$

Here $\sigma_t = 0.7$ stands for the turbulent Prandtl/Schmidt number.

2.2.2 Solid Phase

As is shown in Figure 1 part of the bed volume is occupied by solid particles. A distribution can be described by a value referred to as porosity P which is the ratio of void to total volume.

$$P = \frac{V_{void}}{V_{tot}} \tag{35}$$

Another parameter often used is the void ratio e which is defined as follows.

$$e = \frac{P}{1-P} = \frac{V_{void}}{V_{solid}} \tag{36}$$

These values initially may vary throughout the bed, and in time will change due to combustion and the motion of particles. Therefore the solid phase is assumed as a three-dimensional unsteady motion of incompressible particles. Friction forces act between particles during motion depending on the stress applied normal to the contact surface as shown in Figure 2.

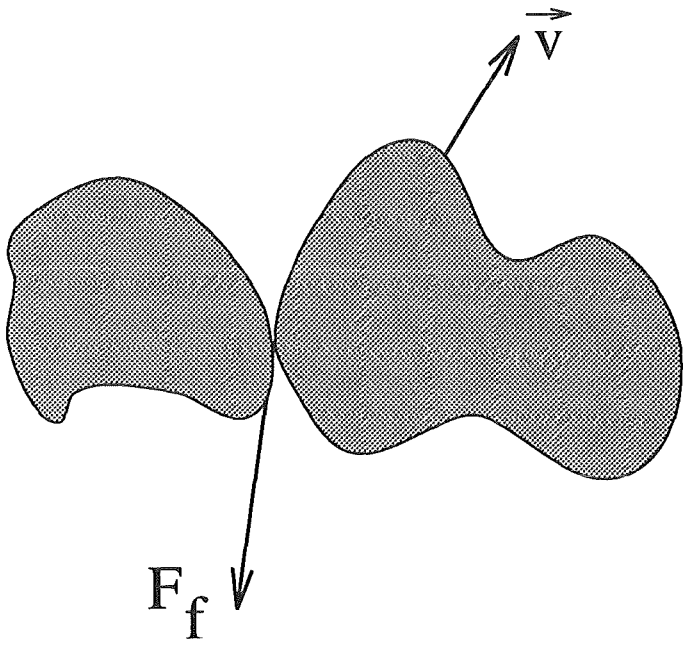

Figure 2: Friction forces at particle contacts

Furthermore momentum transfer at the phase boundaries and the impacts of gas phase forces on particles are negligible.

In order to resolve different properties within a particle a very fine mesh would be necessary which in turn would lead to unreasonable high CPU times for the present application. However, information about the inner-particle distributions of e.g. temperature or mass fractions is still desirable; this is why a subgrid modelling was employed. This

feature combines the advantage of a detailed description of variables inside the particle with reduced CPU time, reinforced by an implicit algorithm. Hence a set of of coupled non-linear differential equations for mass, momentum, energy and species follow.

Continuity:

$$\rho_s \nabla \cdot ((\mathbf{v_s} - \mathbf{v_B})) = S_s \tag{37}$$

where ρ_s and v_s are the solid phase density and velocity respectively The right hand side represents the effects of devolatilization and heterogeneous combustion.

Momentum:

$$\rho_s \frac{\partial \mathbf{v_s}}{\partial t} + \rho_s \nabla \cdot ((\mathbf{v_s} - \mathbf{v_B})\mathbf{v_s}) = -\nabla \cdot \bar{\sigma} - \nabla \cdot \bar{\tau_f} \tag{38}$$

where $\bar{\sigma}$ and $\bar{\tau_f}$ stand for the normal and shear stress tensor within a packed bed. The particular appearance of the right hand side was derived on the basis that as mentioned above in the "Experimental Programm" section stresses such as σ_x and σ_y can be expressed by σ_z and proportionality constant k_a.

$$\sigma_x = \sigma_y = k_a \sigma_z \tag{39}$$

Shear stresses due to friction are related to normal stresses σ_n by a friction coefficient μ_f.

$$\tau_f = \mu_f \sigma_n \tag{40}$$

Hence the decomposed stress tensor will look as written below.

$$\bar{\sigma} + \bar{\tau} = \sigma_z \begin{pmatrix} k_a & 0 & 0 \\ 0 & k_a & 0 \\ 0 & 0 & 1 \end{pmatrix} + k_a \mu_f \sigma_z \begin{pmatrix} 0 & 1 & 1 \\ 1 & 0 & 1 \\ 1 & 1 & 0 \end{pmatrix} \tag{41}$$

On the assumption that a particle motion can occur only when the forces applied F_i exceed the friction forces,

$$F_i > \sum_{i \neq j} \tau_{ji} A_i \tag{42}$$

where A_i is the surface area on which the shear stress τ_{ji} acts. Finally the shear stress tensor takes the following form.

$$\bar{\tau} = \begin{cases} 0 & \text{if } F_i \leq \sum_{i \neq j} \tau_{ji} A_i \\ \sum_{i \neq j} \tau_{ji} & \text{if } F_i > \sum_{i \neq j} \tau_{ji} A_i \end{cases} \tag{43}$$

Analogous to conditions in the gas phase the gas phase a transport equation for various

species is solved for the solid phase as products emerge due to devolatilization and heterogeneous combustion. The same applies to the water content of municipal waste material, which evaporates into the gas phase.

Species:

$$\rho_s \frac{\partial Y_{i,s}}{\partial t} + \rho_s \nabla \cdot ((\mathbf{v_S} - \mathbf{v_B}) Y_{i,s}) = \nabla \cdot (D_{i,s} \nabla Y_{i,s}) + S_{Y_{i,s}} \tag{44}$$

where $Y_{i,s}$ is the mass fraction of species i of the solid phase.

To derive the energy equation convective heat transfer between gas and solids and conduction within the particle is assumed. Contrary to conditions in the gas phase radiation is important and is employed as diffuse radiation between particles with reflection and adsorption properties. Thus the equation describing energy transfer between two particles at the temperatures T_i and T_j reads as follows.

$$Q_{i \to j} = A_i F_{i \to j} \frac{\sigma (T_i^4 - T_j^4)}{\frac{1}{\epsilon_i} + \frac{1}{\epsilon_j} - 1} \tag{45}$$

where σ and ϵ denote the Stefan-Boltzmann constant ($\sigma = 5.6696\, 10^{-8}\ W/(m^2 K^4)$) and the emissivity respectively. A_i and $F_{i \to j}$ stand for the surface area of particle i and the dimensionless view factor, which represents the fraction of radiation leaving A_i that is directly intercepted by A_j. Here the view factors, which are very difficult to calculate at times, may be estimated by a surface-weighted scheme of neighbouring spherical particles with radius r as given below.

$$F_{i \to j} = \frac{r_i^2}{\sum_{j=1}^{n} r_j^2} \tag{46}$$

Together with the divergence of Equation 45 energy will be conserved as described in the following equation.

Energy:

$$\rho_s \frac{\partial e_s}{\partial t} + \rho_s \nabla \cdot ((\mathbf{v_S} - \mathbf{v_B}) e_s) = \nabla \cdot (\lambda_s \nabla T_s) + \nabla \cdot q_r + \Gamma_s \tag{47}$$

where λ_s and q_r denote the heat conductivity of particles and the radiative flux. The source term Γ_s summarises effects such as heat transfer between gas and particles, dissipation due to friction and heat generation due to heterogeneous combustion.

Information and data on the physical composition of solid wastes are important for both modelling and assessing the feasibility of resource and energy recovery. Although the percentages of municipal waste components vary with the location, season, economic conditions and many other factors the data reported in the tables 5, 6, 7, 8 below have proved to be adequate in characterizing solid waste for most applications [23], [36], [37], [32].

Component	% by weight
Food wastes	15
Paper	40
Cardboard	4
Plastics	3
Textiles	2
Rubber	0.5
Leather	0.5
Garden trimmings	12
Wood	2
Glass	8
Tin cans	6
Nonferrous metals	1
Ferrous metals	2
Dirt, ashes, brick, etc	4

Table 5: Typical physical composition of municipal solid waste

A very good and representative analysis of municipal waste material for Germany is reported in Table 9 (Bundesweite Hausmüllanalyse 1985). Based on these data relevant properties of waste material may be evaluated as mass-averaged values from the properties of its components.

For ash usually these properties are assumed: $\lambda = 0.93\ W/mK$, $\rho = 1307\ kg/m^3$, $c_p = 808 - 2000\ J/kgK$.

As stated above within the assumptions subgrid modelling was proposed, which will be described in detail in the section below. Solving the set of differential equations yields a volume-averaged quantity for the solid phase. However, since devolatilization and combustion to a large extent are surface-related processes averaged values are no satisfactory estimates of surface regions to describe the relevant aspects. In order to compensate for this disadvantage a method is derived which provides a distribution across a particle for the necessary variables. Therefore a preliminary assumption about the geometric appearance of a particle has to be made. As municipal waste material contains a variety of particle shapes the influence of extreme volume-to-surface ratios on surface or pore effectiveness was first investigated as shown in Figure 3.

The Thiele-module expresses a ratio between a chemical and a diffusion time-scale, whereas the effectiveness factor defines in how far an available surface area is made use of in relation to these processes occurring on a particle surface. Although the lines for flat, long cylindrical and spherical particles cover a wide range of volume-to-surface ratios the difference in effectiveness factors turns out to be moderate, thus justifying the assumption of a spherical geometry representing various shapes. Furthermore the behaviour is assumed to be one-dimensionally unsteady with diffusive transport and adsorption and desorption approximated by Langmuir's isotherm. The differential equation in spherical coordinates for any conserved scalar Θ thus is described by the following equation.

Component (% by weight)	Carbon	Hydrogen	Oxygen	Nitrogen	Sulfur	Ash
Food wastes	48	6.4	37.6	2.6	0.4	5.0
Paper	43.5	6.0	44.0	0.3	0.2	6.0
Cardboard	44	5.9	44.6	0.3	0.2	5
Plastics	60	7.2	22.8			10
Textiles	55	6.6	31.2	4.6	0.15	2.5
Rubber	78	10		2		10
Leather	60	8	11.6	10	0.4	10
Garden trimmings	47.8	6	38	3.4	0.3	4.5
Wood	49.5	6	42.7	0.2	0.1	1.5
Dirt, ashes, brick, etc	26.3	3	2	0.5	0.2	68

Table 6: Combustible components in municipal solid wastes

Component	% by weight
Carbon	26
Sulfur	0.5
Fluorine	0.02
Chlorine	0.7
Iron	7
Copper	0.04
Zinc	0.1
Lead	0.08
Cadmium	0.001
Mercury	0.0004

Table 7: Typical composition of municipal solid waste

$$\frac{\partial \Theta}{\partial t} = D' \frac{\partial^2 \Theta}{\partial r^2} + D' \frac{2}{r} \frac{\partial \Theta}{\partial r} - k\Theta \tag{48}$$

where k is a proportionality constant for an arbitrary source term. The diffusion coefficient D' is derived from the equivalent one in the gas phase, the porosity and tortuosity of paths taken into account in a tortuosity factor T.

$$D' = D_g \frac{P}{T} \tag{49}$$

The solution to Equation 48 yields a distribution of relevant variables e.g. temperature and species over sphere radius. The appropriate rates for devolatilization and heterogeneous combustion will be modelled by Arrhenius equations where the combustion of

Enthalpy MJ/kg	Water %	Combustible %	Carbon %	Hydrogen %	Oxygen %	Nitrogen %	Sulfur %
6-10	25-30	40-50	20-25	2-5	10-20	0.5	0.5

Table 8: Properties of municipal solid wastes

Component	Fraction % by weight	Comb. Enthalpy kJ/kg	weighted Comb. Enth. kJ/kg
Paper	12.0	16000	1920
Cardboard	4.0	15000	600
Tetra pak	1.9	15000	285
Ferrous metals	2.8	0	0
Nonferrous metals	0.4	0	0
Glas	9.2	0	0
Plastics	5.4	30000	1620
Textiles	2.0	18000	360
Minerals	2.0	0	0
Garden trimmings	29.9	4500	1345
Hazardous waste	0.4	4000	15
Waste material (8-40 mm)	16.0	4000	640
Waste material (< 8 mm)	10.1	4000	400
Miscellaneous	3.9	4500	175
Total	100		7360

Table 9: Composition of municipal waste material in Germany

waste material represented by a carbon-hydrogen combination in a first approach is approximated by a one-step reaction.

$$C_nH_m + (n + m/4)O_2 = nCO_2 + m/2H_2O \tag{50}$$

A reaction rate can be written as follows.

$$\frac{dc_s}{dt} = kc_s c_{O_2,ad} \tag{51}$$

where k denotes a frequency factor and c_s and $c_{O_2,ad}$ are concentrations of solid phase and of on surface adsorbed oxygen.

Similarly an adsorption process can be described by a reaction of a gaseous molecules $c_{i,g}$ with active sites c_{as} on a surface to form an adsorbed state $c_{i,ad}$.

$$c_{i,g} + c_{as} = c_{i,ad} + c_{as} \tag{52}$$

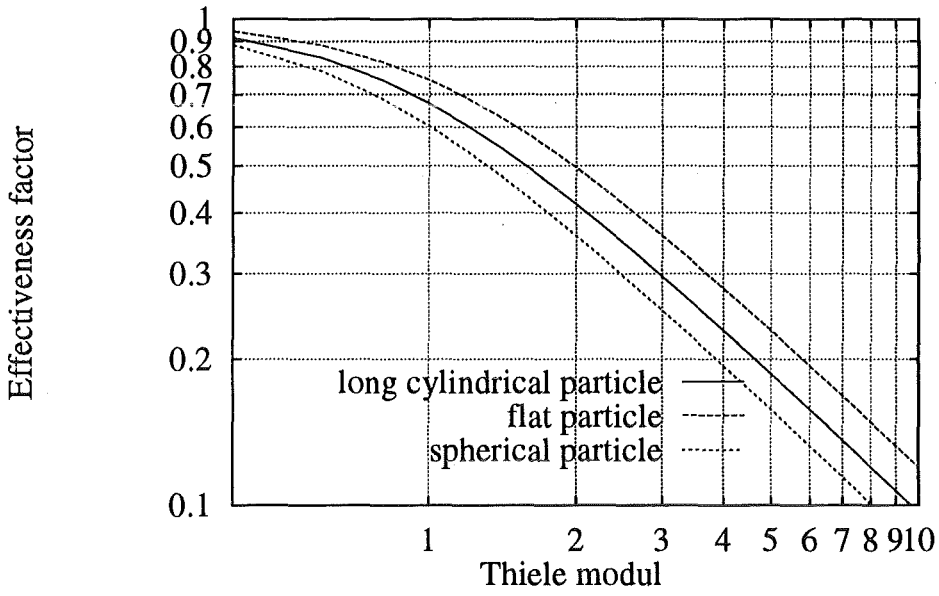

Figure 3: Effectiveness factor over Thiele-modul

As in the present approach none of the active sites is in any way distinguished from other locations it may be replaced by the concentration of the solid phase and provides the following adsorption rate.

$$\frac{dc_{c_{i,ad}}}{dt} = k_{ad} c_{i,g} (c_s - c_{i,ad}) \tag{53}$$

The same scheme applied to desorption with the the following reaction scheme

$$c_{i,ad} = c_{i,g} \tag{54}$$

yields a desorption rate

$$\frac{dc_{c_{i,g}}}{dt} = k_{des} c_{i,ad} \tag{55}$$

Together with the formula of the Langmuir isotherm which assumes an equilibrium between the adsorption and desorption rates and is valid for many technical applications the following expression is obtained for the concentration of the adsorbed species.

$$c_{i,ad} = \frac{k_{ad} c_{i,g} c_s}{k_{ad} c_{i,g} + k_{des}} \tag{56}$$

Substituting $c_{i,ad}$ in Equation 51 by Equation 56 furnishes.

$$\frac{dc_s}{dt} = k\frac{k_{ad}c_{i,g}c_s^2}{k_{ad}c_{i,g} + k_{des}} \tag{57}$$

which defines a burning rate for particles and can be validated by experimental data with the set of equations mentioned above.

In a second step Equation 50 could be substituted for the following reaction scheme.

$$C + H_2O \rightarrow CO + H_2 \tag{58}$$

$$C + \frac{1}{2}O_2 \rightarrow CO \tag{59}$$

$$C + CO_2 \rightarrow 2CO \quad (Boudard's\ reaction) \tag{60}$$

$$H_2 + \frac{1}{2}O_2 \rightarrow H_2O \tag{61}$$

which provides more detailed information about the system.

2.3 Discretisation Method and Solution Algorithm

Within the method a two- or three-dimensional domain is subdivided into non-overlapping control-volumes with an arbitrary number of faces as shown in Figure 4.

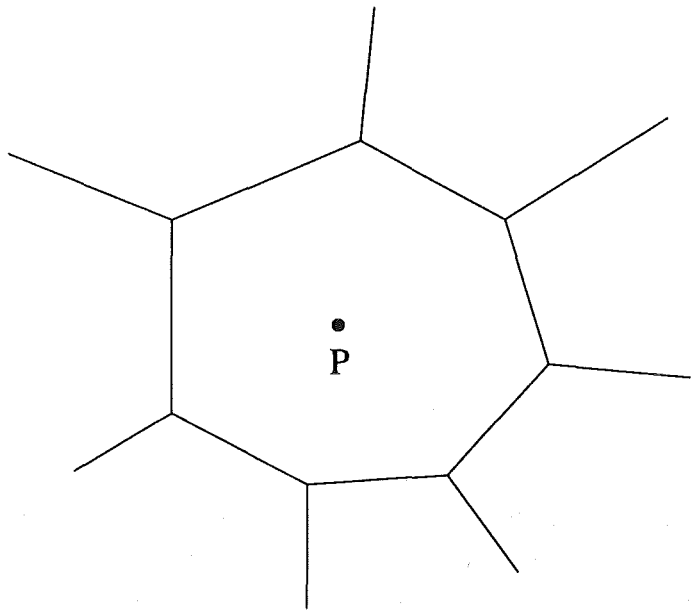

Figure 4: Control-volume

Arbitrarily orientated faces are plane and have one or more edges in common. The mesh is unstructured and therefore needs an additional addressing scheme. However, this

disadvantage is more than compensated for by mesh-refinement, which can be applied locally, as opposed to all-over refinement for structured meshes and by an interface easy to handle for any mesh generator of the finite-volume or finite-element types.

Each of the volumes encloses a grid node, labelled P in Figure 4, at which scalar quantities such as pressure, temperature, density and mass fraction together with the velocity as a vector quantity are calculated. One of the most attractive features of this formulation is its obeying the integral conservation of quantities like mass, momentum and energy at each cell and therefore over the whole domain. Nodal values of the unknown quantities are obtained by integrating over the control-volume in space and time. The spatial differences are approximated by a hybrid upwind/central differencing scheme. Both an explicit and an implicit Euler scheme for temporal discretisation were chosen for reasons of simplicity. The SIMPLER/PISO algorithm, which is of a predictor/corrector type, is employed to yield a solution of the coupled conservation equation for mass, energy and momentum. For further reference see [63], [30], [29].

2.4 Initial and Boundary Conditions

For the test cases described later in this paper a set of initial conditions is required for both the gas phase and the particles. Specified temperatures and pressures, which may be assigned individually to each cell, are sufficient for the gas flow, while the solid phase requires additional information, among which is the distribution of particles namely porosity together with the composition specified by the mass fractions of carbon, water and volatiles.

For the fluid-to-particle heat transfer coefficient $h_{g\to s}$ an empirical correlation has to be selected from a range of existing experimental results. These empirical correlations, which were presented in terms of Colburn-Chilton factors j_h, can be expressed in the following form [5].

$$j_h = 0.91 Re^{-0.51} \psi \quad (Re < 50) \tag{62}$$

$$j_h = 0.61 Re^{-0.41} \psi \quad (Re > 50) \tag{63}$$

Here the Colburn-Chilton factor j_h and the Reynolds number are defined by

$$\begin{aligned} j_h &= \frac{h_{g\to s}}{c_p \rho \mathbf{v}} \left(\frac{c_p \mu}{\lambda} \right)_f^{2/3} \\ &= Nu Re^{-1} Pr^{-1/3} \end{aligned} \tag{64}$$

$$Re = \left(\frac{\rho \mathbf{v}}{a \mu \psi} \right)_f \tag{65}$$

In these equations the subscript f denotes properties evaluated at the "film temperature"

$T_f = 1/2(T_s + T_g)$. The quantity ψ is an empirical coefficient depending on the particle shape ($\psi = 1$ for spheres). The heat-transfer equation between the gas and the solid phases now takes the following form.

$$dQ = h_{g \to s} a V (T_s - T_g) \tag{66}$$

in which V is the bed volume (solid plus gas) and a is the solid particle surface area per unit bed volume.

Mass transfer coefficients are obtained by analogy with the corresponding laws of heat transfer and thus result in the following expression for the Colburn-Chilton factor j_d.

$$\begin{aligned} j_d &= \frac{k_{g \to s}}{c\mathrm{v}} \left(\frac{\mu}{\rho D} \right)_f^{2/3} \\ &= ShRe^{-1}Sc^{-1/3} \end{aligned} \tag{67}$$

where c and D stand for the concentration of a species and the diffusion coefficient respectively and $k_{g \to s}$ denotes the mass transfer coefficient.

A similar relationship for the mass transfer was developed by Smith et al [21], whose validity for the present problem will be evaluated.

$$Sh = 0.221 Re^{0.564} Sc^{1/3} \tag{68}$$

For the boundary conditions a mass flux of combustion air has to be given and equally a radiative flux onto the particles, which is obtained from calculations in the entire combustion chamber.

2.5 Summary

Within this study a finite-volume method to simulate flow and combustion phenomena of a furnace for municipal waste material was developed. The gas flow, motion of particles, temperature distribution in conjunction with the evaporation of water, devolatilization and combustion are described by their respective conservation equations, which yields the distribution of the relevant variables i.e. velocity, temperature, pressure and species for the gas phase and the particle phase within a packed bed.

In a first application the method will be validated by experiments carried out with the KLEAA laboratory furnace. The one-dimensional character of the experiments allows the flow and temperature regime and more importantly the devolatilization rate of different species and combustion behaviour to be evaluated. Hence comparison with experiments will lead to a fast and effective validation procedure before calculations begin in TAMARA, a small-scale furnace of commercial appearance. Comparison with experimental results will emphasize the three-dimensional character of the practical application of the simulation method and thus proves its suitability for further application and design studies.

References

[1] Bejan A. *Convection Heat Transfer.* John Wiley & Sons, 1984.

[2] Levendis Y. A., Flagan R. C., and Gavalas G. R. *Combust. Flame*, 76:221, 1989.

[3] Taylor H. A. and Thon N. *Journal Am. Chem. Soc.*, 74(4):4169, 1952.

[4] Anthony D. B., Howard J. B., Hottel H. C., and Meissner H. P. Rapid devolatilization of pulverized coal. *Symp. Int. Combust. Proc.*, 15:475, 1977.

[5] Bird R. B., Stewart W. E., and Lightfoot E. N. *Transport Phenomena.* John Wiley & Sons, 1960.

[6] Edelman R. B. and Fortune O. F. A quasi-global chemical kinetic model for the finite rate combustion of hydrocarbon fuels with application to turbulent burning and mixing in hypersonic engines and nozzles. *AIAA Pa.*, 69-86, 1969.

[7] Fu W. B. and Zhang E. Z. A universal correlation between the heterogeneous ignition temperatures of coal char particles and coals. *Combustion and Flame*, 90:103–113, 1992.

[8] Howard J. B., Williams G. C., and Fine D. H. Kinetics of carbon monoxide oxidation in postflame gases. In *14th Symposium (Int.) Combustion*, pages 975–986, 1972.

[9] Howard J. B. and Essenhigh R. H. Mechanism of solid-particle combustion with simultaneous gas-phase volatiles combustion. In *11. Symp. Combustion*, pages 399–408, 1967.

[10] Bansal R. C., Vastola F. J., and Walker P. L. *Journ. Carbon*, 8:197, 1970.

[11] Chen J. C. PhD thesis, University Michigan, Ann Arbor, 1961.

[12] Chen J. C. and Churchill S. W. Radiant heat transfer in packed beds. *A. I. Ch. E. Journal*, 9:35–41, 1963.

[13] Ward J. C. Turbulent flow in porous media. *J. Hydraul. Div. ASCE*, 90:1–12, 1964.

[14] Gray D., Cogoli J. G., and Essenhigh R. H. Problems in pulverized coal and char combustion. *Adv. Chem. Ser.*, 131(6):72, 1976.

[15] Low M. J. D. *ACS Chem. Rev.*, 60(3):267, 1960.

[16] Vortmeyer D. Wärmestrahlung in dispersen Feststoffsystemen. *Chem. Ing. Tech.*, 51:839–851, 1979.

[17] de Soete G. G. *Rev. Inst. Franc. Petr.*, 37:403–530, 1982.

[18] di Blasi C., Crescitelli S., Russo G., and Cinque G. Numerical model of ignition process of polymeric materials including gas-phase absorption of radiation. *Combustion and Flame*, 83:333–344, 1991.

[19] Specht E. *Kinetik der Abbaureaktionen.* PhD thesis, Technische Universität Clausthal, 1993.

[20] DeSoete G. G. Overall reaction rates of NO and N_2 formation from fuel nitrogen. *Symp. (Int.) Combust.*, 15:1093, 1975.

[21] Smith III F. G., Pendarvis R. W., and Rice R. W. Combustion of cellulosic char under laminar flow conditions. *Combustion and Flame*, 88:61–73, 1992.

[22] Tchobanoglons G., Theisen H., and Eliassen R. *Solid Wastes.* McGraw Hill Inc, 1983.

[23] Ychobanoglous G. and Theisen H. *Solid Waste: Engineering and Management Issues.* McGraw Hill Book Company, 1977.

[24] Brauer H. *Stoffaustausch einschließlich chemischer Reaktionen.* Verlag Sauerländer, 1971.

[25] Essenhigh R. H. *Chemistry of Coal Utilization*, chapter Fundamentals of Coal Combustion, page 1153. Wiley, New York.

[26] Essenhigh R. H., Isra M. K., and Shaw D. W. Ignition of coal particles: A review. *Combustion and Flame*, 77:3–30, 1989.

[27] Juntgen H. and van Heek K. H. *Fuel Proc. Technol.*, 2:261–293, 1979.

[28] Kobayashi H., Howard J. B., and Sarofin A. F. Coal devolatilization at high temperatures. *Symp. Int. Combust. Proc.*, 16:411, 1977.

[29] Issa R. I. Solution of implicitly discretised fluid flow equations by operator splitting. *Journal of Computational Physics*, 62:40–65, 1986.

[30] Issa R. I., Gosman A. D., and Watkins A. P. The computation of compressible and incompressible recirculating flows by a non-iterative implicit scheme. *Journal of Computational Physics*, 62:66–82, 1986.

[31] Siminski V. J., Wright F. J., Edelman R. B., Economics C., and Fortune O. F. Research on methods of improving the combustion characteristics of liquid hydrocarbon fuels. AFAPL TR 72-74 Vol. I and II, Air Force Aeropropulsion Laboratory, Wright Patterson Air Force Base, Ohio, 1972.

[32] Thome-Kozmiensky K. J. *Systeme und Müllverbrennung*, chapter Müllverbrennung und Rauchgasreinigung. EF-Verlag Berlin, 1983.

[33] Yang J.-T. and Wang G.-G. The effect of heat transfer on coal devolatilization. *Journal of Heat Transfer*, 112:193–200, 1990.

[34] Chan C. K. and Tien C. L. Radiative transfer in packed spheres. *Journal of Heat Transfer*, February:52–58, 1974.

[35] Edwards D. K. *Radiation Heat Transfer Notes.* Hemisphere Publishing Corporation, 1981.

[36] Görner K. *Technische Verbrennungssysteme.* Springer Verlag, 1991.

[37] Sattler K. and Emberger J. *Behandlung fester Abfälle.* Vogel Buchverlag, 1992.

[38] Vafai K. and Sozen M. Analysis of energy and momentum transport for fluid flow through a porous bed. *Journal of Heat Transfer*, 112:690–699, 1990.

[39] Hunt M. L. and Tien C. L. Non-darcian convection in cylindrical beds. *Journal of Heat Transfer*, 110:378–384, 1988.

[40] Botterill J. S. M. *Fluid-Bed Heat Transfer.* Academic Press, 1975.

[41] Kanury A. M. *Introduction to Combustion Phenomena.* Gordon and Breach Science Publisher, 1975.

[42] Kimber G. M. and Gray M. D. Rapid devolatilization of small coal particles. *Combustion and Flame*, 11:360, 1967.

[43] Laurendeau N. M. Heterogeneous kinetics of coal char gasification and combustion. *Prog. Energy Combust. Sci.*, 4:221, 1978.

[44] Loewenberg M. and Levendis Y. A. Combustion behaviour and kinetics of synthetic and coal-derived chars: Comparison of theory and experiment. *Combustion and Flame*, 84:47–65, 1991.

[45] Schuberg E. M., Peters W. A., and Howard J. B. Product compositions and formation kinetics in rapid pyrolysis of pulverized coal - implications for combustion. *Symp. Int. Combust. Proc.*, 17:177, 1979.

[46] Hautman A. N., Dryer F. L., Schlug K. P., and Glassman I. A multiple-step overall kinetic mechanism for the oxidation of hydrocarbons. *Combust. Sci. Technol.*, 25:219, 1981.

[47] Laraqui N. and Bransier J. Détermination du débit de pyrolyse de matériaux solides soumis à un flux de chaleur radiatif, Partie II: Modélisation numérique. *Rev. Gèn. Therm. Fr.*, No. 315-316:192–198, 1988.

[48] Semenov N. N. *Z. Physik*, 48:571, 1928.

[49] Zehner P. *Experimentelle und theoretische Bestimmung der effektiven Wärmeleitfähigkeit durchströmter Kugelschüttungen bei mäßigen und hohen Temperaturen.* VDI-Verlag, 1973.

[50] Walker P.L., Rusinko F., and Austin L. G. Gas reactions of carbon. *Adv. Catal.*, 11:135, 1959.

[51] Blake T. R. and Libby P. A. Combustion of a spherical carbon particle in slow viscous flow. *Combustion and Flame*, 86:147–161, 1991.

[52] Howell J. R. Thermal radiation in participating media: The past, the present and some possible futures. *Journal of Heat Transfer*, 110:1220–1229, 1988.

[53] Khan M. R., Everitt C. E., and Lui A. P. Modeling of oxygen chemisorption kinetics on coal char. *Combustion and Flame*, 80:83–93, 1990.

[54] Siegel R. and Howell J. R. *Thermal Radiation Heat Transfer.* Hemisphere Publishing Corporation, 1981.

[55] Thurgood J. R. and Smoot L. D. *Volatiles Combustion.* 1979.

[56] Viskanta R. and Mengüç M. P. Radiation heat transfer in combustion systems. *Prog. Energy Combust. Sci.*, 13:97–160, 1987.

[57] Engleman U. S. Survey and evaluation of kinetic data of reactions in methane/air combustion. EPA-600/2-76-003, Exxon Research and Engineering Co., Linden, New Jersey, 1976.

[58] Niksa S. and Lau C.-W. Global rates of devolatilization for various coal types. *Combustion and Flame*, 94:293–307, 1993.

[59] Wichman I. S. and Atreya A. A simplified model for the pyrolysis of charring materials. *Combustion and Flame*, 68:231–247, 1987.

[60] Kashiwagi T. A radiative ignition model of a solid fuel. *Combustion Science and Technology*, 8:225–236, 1974.

[61] Kashiwagi T. Radiative ignition mechanism of solid fuels. *Fire Safety Journal*, 3:185–200, 1981.

[62] Grigull U. *Die Grundgesetze der Wärmeübertragung.* Springer Verlag, 1963.

[63] Patankar S. V. *Numerical Heat Transfer and Fluid Flow.* McGraw-Hill Book Company, 1980.

[64] Petrella R. V. The mass burning rate of polymers, wood and organic liquids. *Journal of Fire and Flammability*, 11:3–21, 1978.

[65] Shkandinsky K. V., Shkadinskaya G. V., and Matkowsky B. J. Self-compaction or expansion in combustion synthesis of porous materials. *Combust. Sci. and Tech.*, 88:271–292, 1992.

[66] Bartok W. and Sarofim A. F. *Fossil Fuel Combustion.* John Wiley & Sons, 1991.

[67] Smith I. W. The combustion rates of coal chars: A review. *Symp. (Int.) Combust. [Proc.]*, 19:1045, 1983.